Imaging properties of phase-shifting apodizers

A. Sauceda[a], P.J. García Ramírez[a], L. García-González[a],
J. Martínez-Castillo[a], L. Herrera-May[a], and A. Castro[b]
[a]*Centro de Investigación en Micro y Nanotecnología de la Universidad Veracruzana,*
Fracc. Costa Verde, Veracruz, ZC. 94292 Ver., México,
e-mail: asauceda@uv.mx, jagarcia@uv.mx
leagrarcia@uv.mx, jaimartinez@uv.mx, leherrera@uv.mx
[b]*Instituto Nacional de Astrofísica, Óptica y Electrónica,*
Apartado Postal 216 Puebla 72000, Puebla, Mexico,
e-mail: betina@inaoep.mx

Recibido el 7 de marzo de 2006; aceptado el 9 de agosto de 2006

We discuss the imaging properties of Phase Shifting Apodizers (PSAs) in terms of their Optical Transfer Function (OTF). The capability to transfer spatial frequencies from the input to the output of an optical imaging system, in the presence of focus error, is quantified by inspecting the three-dimensional Modulation Transfer Function (3D-MTF). We have found that, in the search of novel apodizers for increasing the focal depth in imaging optical systems, it is not sufficient to analyze the axial impulse response of that system. Some apodizers, even when they increase the focal depth along the optical axis, provide poor imaging properties with respect to defocus. Yet we identify specific values for some important parameters of the PSA that allow us to achieve high focal depth without severally sacrificing the optical performance of the system. We present computer simulations of the 3D-MTF of the system that incorporates these apodizers as well as the output images that can be obtained with it.

Keywords: Phase-shifting apodizer; optical transfer function; image formation.

Discutimos las propiedades de formación de imágenes de los apodizadores de cambio de fase (o PSA, por sus siglas en inglés) en términos de la Función de Transferencia Óptica (OTF, por sus siglas en inglés). Su capacidad para transferir frecuencias espaciales de la entrada hacia la salida de un sistema óptico, en presencia del error de desenfocamiento, es cuantificada inspeccionando el módulo de la OTF tridimensional (3D-MTF). Hemos encontrado que, en sistemas ópticos que forman imágners, el desempeño óptico de un nuevo apodizador, no se garantiza con el análisis de la respuesta al impulso axial del sistema. En el caso algunos apodizadores, aún cuando incrementan la profundidad focal a lo largo del eje óptico, su capacidad para formar imágenes está muy deteriorada. Aún así, identificamos valores específicos de los parámetros importantes en los PSA, que nos permiten conseguir alta profundidad focal, sin sacrificar significativamente el desempeño óptico del sistema. Presentamos simulaciones por computadora de las 3D-MTFs del sistema óptico que incorpora estos apodizadores, así como también las imágenes de salida que pueden ser obtenidas con éstos.

Descriptores: Apodizadores de cambio de fase; función de transferencia óptica; formación de imágenes.

PACS: 42.15.Eq; 42.30.Lr; 42.30.Va

1. Introduction

Phase Shifting Apodizers (PSAs) play an important role in photolithography, microscopy and other applications where high optical resolution is required, as for example: high-density optical data storage or specific purpose imaging systems. PSAs, originally proposed for improving optical resolution in photolithography [1], have been widely described from the point of view of lithography applications. Different works focusing on their optimization and their fabrication have been reported [2,3]. Some others have performed computer simulations for lithography projection systems with emphasis onto their optical performance under specific conditions [4,5]. PSAs with three or more portions have also been proposed for increasing the recording density in optical disks [6-8]. Recently, a method for tuning the three-dimensional intensity distribution with applications in electro-optical focusing systems and in optical trapping, by changing geometrical parameters in a PSA, was proposed [9].

In the aforementioned works, the optical properties of PSAs have been described, emphasizing the capabilities of PSAs to increase the focal depth. This is done without analyzing the shape of their associated MTF. However, as we shall show, their associated MTF reveals that they are not suitable for optical imaging purposes. Even so, we show that, by changing the geometrical parameters as in Ref. 9, we can optimize the PSAs so that their imaging properties will be suitable in optical imaging applications.

From the point of view of optical image formation, the use of the optical transfer function (OTF) for describing linear optical systems represents a valuable tool, because we can quickly and easily evaluate the optical performance of the system. Although both the spatial domain and the frequency domain are equivalent in describing the optical performance of linear optical systems, we must be aware that it is possible synthesize apodizers with an apparently good axial point spread function (PSF) that are however not suitable for image formation, as can be seen by analyzing the corresponding OTF.

In this work we perform an analysis of PSAs by inspecting their MTF and their axial PSF in order to find a suitable

apodizer for imaging applications. We believe our work complements the work reported by other authors, who analyze PSAs from the point of view of PSF. We show for the first time numerical simulations of the associated MTF for phase-shifting apodizers.

In Sec. 2 we describe the axial behavior of the Point Spread Function of the PSAs by using the so-called Pseudo-Cartesian coordinates. Section 3 reviews the fundamental equations that relate the three-dimensional Point Spread Function (3D-PSF) for an incoherent optical system with the defocused optical transfer function. Finally, in Sec. 4 we show numerical simulations of the output images that can be obtained by using a phase-shifting apodizer at the pupil plane of an optical imaging system.

2. The axial impulse response

The amplitude impulse response $p(x,y)$ or Point Spread Function (PSF) of an optical processor, as shown in Fig. 1, is related to the pupil function $\tilde{p}(\nu,\mu)$ by a two-dimensional Fourier transform. That is,

$$p(x,y) = \int_{\nu=-\infty}^{\infty}\int_{\mu=-\infty}^{\infty} \tilde{p}(\nu,\mu)\exp\left[i2\pi\left(x\nu+y\mu\right)\right]d\nu d\mu. \quad (1)$$

However, if we are interested in analyzing the evolution of the PSF along the optical axis, it is then convenient to consider the three-dimensional Point Spread Function 3D-PSF of the optical system, which is given by

$$p(x,y,z) = \int_{\nu=-\infty}^{\infty}\int_{\mu=-\infty}^{\infty} \tilde{p}(\nu,\mu)\exp\left[-i\pi\lambda z\left(\nu^2+\mu^2\right)\right] \times \exp\left[i2\pi\left(x\nu+y\mu\right)\right]d\nu d\mu. \quad (2)$$

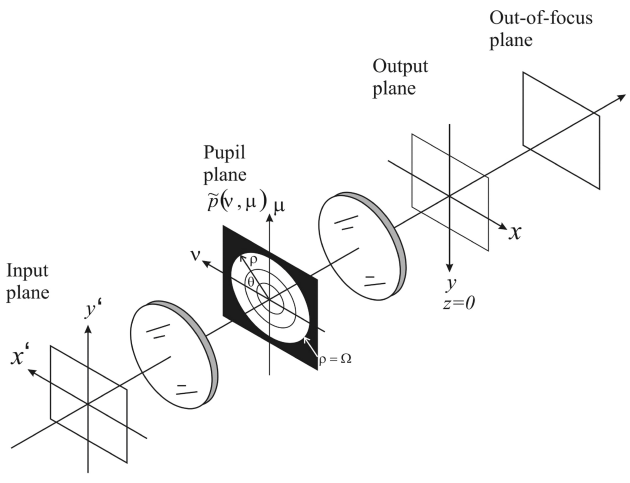

FIGURE 1. Schematic diagram of the optical processor.

That is, the amplitude 3D-PSF is obtained by a two-dimensional Fourier transform of the generalized pupil function [10]. Since we are not interested in any other aberration, the generalized pupil function only considers defocus error. As is customary in image formation, we describe an out-of-focus plane located at a distance z, from the in-focus plane, along the optical axis, by using the wave aberration or defocus coefficient W_{20}. That is,

$$W_{20} = \frac{(\lambda\Omega)^2}{2}z. \quad (3)$$

The symbol Ω represents the maximum spatial frequency extension of the pupil function, and λ denotes the wavelength of the radiation.

From Eq. (2) we can directly obtain the axial PSF as

$$p(0,0,z) = \int_{\nu=-\infty}^{\infty}\int_{\mu=-\infty}^{\infty} \tilde{p}(\nu,\mu)\exp\left[-i\pi\lambda z\left(\nu^2+\mu^2\right)\right]d\nu d\mu \quad (4)$$

or equivalently, in terms of the defocus coefficient,

$$p(0,0,W_{20}) = \int_{\nu=-\infty}^{\infty}\int_{\mu=-\infty}^{\infty} \tilde{p}(\nu,\mu) \times \exp\left\{-i\frac{2\pi}{\lambda}W_{20}\left[\left(\frac{\nu}{\Omega}\right)^2+\left(\frac{\mu}{\Omega}\right)^2\right]\right\}d\nu d\mu. \quad (5)$$

Now, by use of a suitable change of variables, $\rho^2=\nu^2+\mu^2$, $\nu=\rho\cos\theta$, $\mu=\rho\sin\theta$, $q(z)=p(0,0,z)$, and $\tilde{q}\left(\rho^2,\theta\right)=\tilde{p}(\nu,\mu)$, Eq. (4) can also be written as

$$q(z) = \pi\int_{\rho=0}^{\Omega^2}\left\{\frac{1}{2\pi}\int_{\theta=0}^{2\pi}\tilde{q}\left(\rho^2,\theta\right)d\theta \times \exp\left[-i2\pi\frac{\lambda z}{2}\rho^2\right]\right\}d\rho^2. \quad (6)$$

We can observe in Eq. (6) that the axial behavior of the PSF can also be represented as the one-dimensional Fourier transform, in polar coordinates, of the angular average of a pupil function represented now in the pseudo-Cartesian coordinates $\left(\rho^2,\theta\right)$.

Now, we employ as a pupil the three-portion Phase-Shifting Apodizer schematically represented in Fig. 2a. The phases of the three-portions are 0, π, 0; the radii are ε_1 and ε_2 and Ω. Its equivalent representation, in the pseudo-Cartesian plane, is shown in Fig. 2b, and its mathematical representation is given by

$$\tilde{q}\left(\rho^2,\theta\right)=\left\{rect\left[\frac{\rho^2-\frac{\Omega^2}{2}\varepsilon_1^2}{\Omega^2\varepsilon_1^2}\right]+rect\left[\frac{\rho^2-\frac{\Omega^2}{2}\left(\varepsilon_2^2+\varepsilon_1^2\right)}{\Omega^2\left(\varepsilon_2^2-\varepsilon_1^2\right)}\right]\exp\left(i\pi\right)+rect\left[\frac{\rho^2-\frac{\Omega^2}{2}\left(1+\varepsilon_2^2\right)}{\Omega^2\left(1-\varepsilon_2^2\right)}\right]\right\}rect\left[\frac{\theta-\pi}{2\pi}\right]. \quad (7)$$

Thus, by substituting Eq. (7) in Eq. (6), the axial PSF for the three portions PSA is obtained as

$$q\left(z\right)=\pi\Omega^2\varepsilon_1^2\exp\left[-i\pi\lambda z\frac{\Omega^2\varepsilon_1^2}{2}\right]\ \mathrm{sinc}\left(\frac{\lambda z}{2}\Omega^2\varepsilon_1^2\right)-\pi\Omega^2\left(\varepsilon_2^2-\varepsilon_1^2\right)\exp\left[-i\pi\lambda z\Omega^2\left(\frac{\varepsilon_2^2+\varepsilon_1^2}{2}\right)\right]$$
$$\times\ \mathrm{sinc}\left[\frac{\lambda z}{2}\Omega^2\left(\varepsilon_2^2-\varepsilon_1^2\right)\right]+\pi\Omega^2\left(1-\varepsilon_2^2\right)\exp\left[-i\pi\lambda z\Omega^2\left(\frac{1+\varepsilon_2^2}{2}\right)\right]\ \mathrm{sinc}\left[\frac{\lambda z}{2}\Omega^2\left(1-\varepsilon_2^2\right)\right]. \quad (8)$$

We can easily identify in Eq. (8) the contribution of each portion of the PSA to the axial PSF. The normalized irradiance distribution of the axial PSF is found as the squared modulus of Eq. (8). Figure 3 presents the normalized irradiance distribution for a PSA with different values of the parameters ε_1 and ε_2. It is apparent in all the cases plotted in Fig. 3 that the corresponding PSA's are useful for extending the focal depth. What is more, in some cases the axial impulse response exhibits a flat region near the focus, which is a highly desirable characteristic in an optical imaging system. However, as will be evident in next section, the possibility implementing an optical imaging system with these PSA's is severally restricted. This restriction is mainly due to the loss of contrast in the high frequencies band, as will later be appreciated by inspecting the corresponding 3D-MTF and the corresponding simulated images in Fig. 4.

The first four axial irradiance distributions in Fig. 3 are equivalent to those obtained in Ref. 7. The last combination, ε_1=0.915 and ε_2=1, is the one we present in this work. A PSA with these values represents a two-portion PSA. Even though the normalized axial irradiance distribution of our proposal is equal to the lowest focal depth achieved with a PSA proposed in Ref. 7, we shall show later that the imaging-formation capabilities of our proposal are better than any of the proposals of Ref. 7.

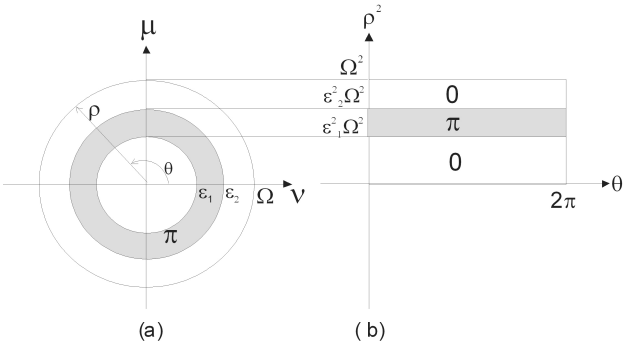

FIGURE 2. Three portion Phase-Shifting Apodizer, (a) in Cartesian coordinates, and (b) pseudo-Cartesian coordinates.

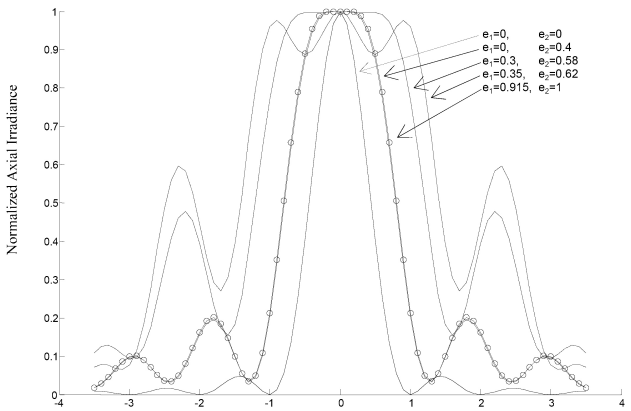

FIGURE 3. Normalized Irradiance of the axial PSF vs. defocus (in W_{20}/λ) for different values of ε_1 andε_2.

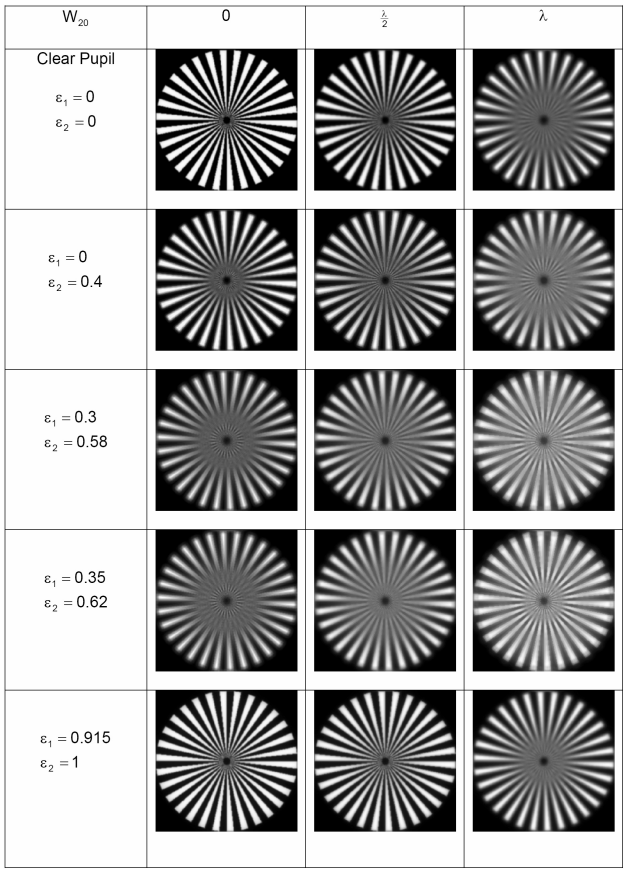

FIGURE 4. Simulated output images.

3. Three dimensional optical transfer function (3D-OTF) for the PSA

In the context of the linear optical systems approach, it is well known that we can analyze optical systems by describing them in the spatial coordinate domain, by means of the point spread function (PSF). Alternatively, we can conveniently go to the frequency domain to visualize the ability of the optical system to transfer spatial-frequency components of the input optical signal toward the output optical signal. In the latter case we are interested in analyzing the Optical Transfer Function (OTF), which is closely related to the PSF by a two-dimensional Fourier Transform [10].

The analysis of a defocused optical system, in the paraxial approximation, was first considered by H.H. Hopkins [11] to suggest the idea of a three-dimensional Optical Transfer Function (3D-OTF). However, the concept of a 3D-OTF was first introduced by Frieden [12] and has been widely described by Sheppard *et al.* for optical systems under different conditions [13-15]. In the present work we use the paraxial three-dimensional point spread function (3D-PSF) to express the 3D-OTF as the autocorrelation of the defocused pupil function, as it was first given by Frieden [12]. That is, by recalling the amplitude 3D-PSF from the previous section, we obtain the corresponding 3D-OTF as the two dimensional Fourier Transform of the squared modulus of Eq. (2). Namely,

$$\tilde{H}(\nu,\mu,z)=\exp\left[-i\pi\lambda z\left(\nu^2+\mu^2\right)\right]\int_{\nu'=0}^{\infty}\int_{\mu'=0}^{\infty}\tilde{q}(\nu',\mu')\,\tilde{q}(\nu'+\nu,\mu'+\mu)\exp\left[-i2\pi\left(\lambda z\nu\nu'+\lambda z\mu\mu'\right)\right]d\nu' d\mu'. \quad (9)$$

The modulus of Eq. (9) corresponds to the three-dimensional Modulation Transfer Function (3D-MTF). Thus, in order to find the 3D-MTF of the pupils depicted in Fig. 2, we digitally construct the pupils, and then we numerically evaluate Eq. (9). Figure 5 shows the 3D-MTF for the PSA's reported in Ref. 7.

For image-formation applications it is highly desirable that the system be able to transfer all spatial frequencies within its passband, as happens in the aberration-free diffraction-limited case (optical system with a clear pupil for the in-focus case). See Fig. 5a. However, as soon as defocus is present, the optical performance of the system drastically decreases because for some values of defocus, specific bands of high frequencies are too attenuated, causing a decrease in the contrast and in the worst case the system cuts some spatial frequencies, losing the image details given for those frequencies. Furthermore, in the zero-valued regions, there is no digital process we can perform in order to recover those rejected spatial frequencies. Figures 5b-d present the 3D-MTF obtained with a system that incorporates the PSAs reported in Ref 7. It is noticeable that, even though the authors reported that the axial behavior of the PSF increases the focal depth, that is, increases the range of non-zero values along the optical axis, their respective transversal MTFs show that the image-formation capabilities are not better than the traditional optical system with the clear pupil. It is apparent from Figs. 5b, 5c and 5d that even for the in-focus case, the 3D-MTF for the analyzed PSA exhibit lower values than the clear pupileven zero-valued regions. This behavior in the 3D-MTF is obvious in the numerically simulated images shown in Fig. 4 and described in Sec. 4.

The 3D-MTF for our proposed PSA is presented in Fig. 6. It is evident from that figure that our proposal presents better image-formation capabilities than the ones proposed in Ref 7. We can see in Fig. 6 that in this case the spatial frequencies shown in 3D-MTF exhibits higher values than those shown in Figs. 5b, 5c, and 5d. However, they have lower values than the clear pupil case Fig. 5a. We remark that our proposed PSA is suitable for imaging purposes since the 3D-MTF in Fig. 5 does not reject any spatial frequency (there are no zero-valued regions) for defocus values less than 1λ.

In the next section we show computer simulations of the output images that can be obtained by using a PSA in the pupil plane of a traditional optical system for different values of the parameters ε_1 and $\varepsilon_2$and for several values of the defocus.

4. Numerical results

In order to find the images that can be obtained with an optical imaging system with a PSA in the pupil plane -see Fig. 1- we numerically compute the following expression:

$$I_{out}(x,y)=\int_{-\infty}^{\infty}\int_{-\infty}^{\infty}\tilde{H}(\nu,\mu;z)\,\tilde{I}_{in}(\nu,\mu)\times\exp\left[i2\pi\left(x\nu+y\mu\right)\right]d\nu d\mu, \quad (10)$$

where I_{out} denotes the irradiance distribution or the output image, $\tilde{I}_{in}$ represents the Fourier spectrum of the input optical signal, and $\tilde{H}(\nu,\mu,z)$ represents the defocused Optical Transfer Function of the optical systems that incorporates the PSA in the pupil plane, given by Eq. (6). As input to the optical system, we use the spoke target.

Qualitatively, we can estimate the optical performance of the PSAs by considering the appearance of the simulated images. The value for a given spatial frequency shown in the 3D-MTFs of Figs. 4 and 5 has a correspondence with the contrast of the image. The spatial frequencies with zero-value will translate into a lack of information in the image. Since all the analyzed PSAs have a circular symmetry, we will identify zero-value regions as gray rings. The fewer the gray rings on the image, the better the PSA for image formation.

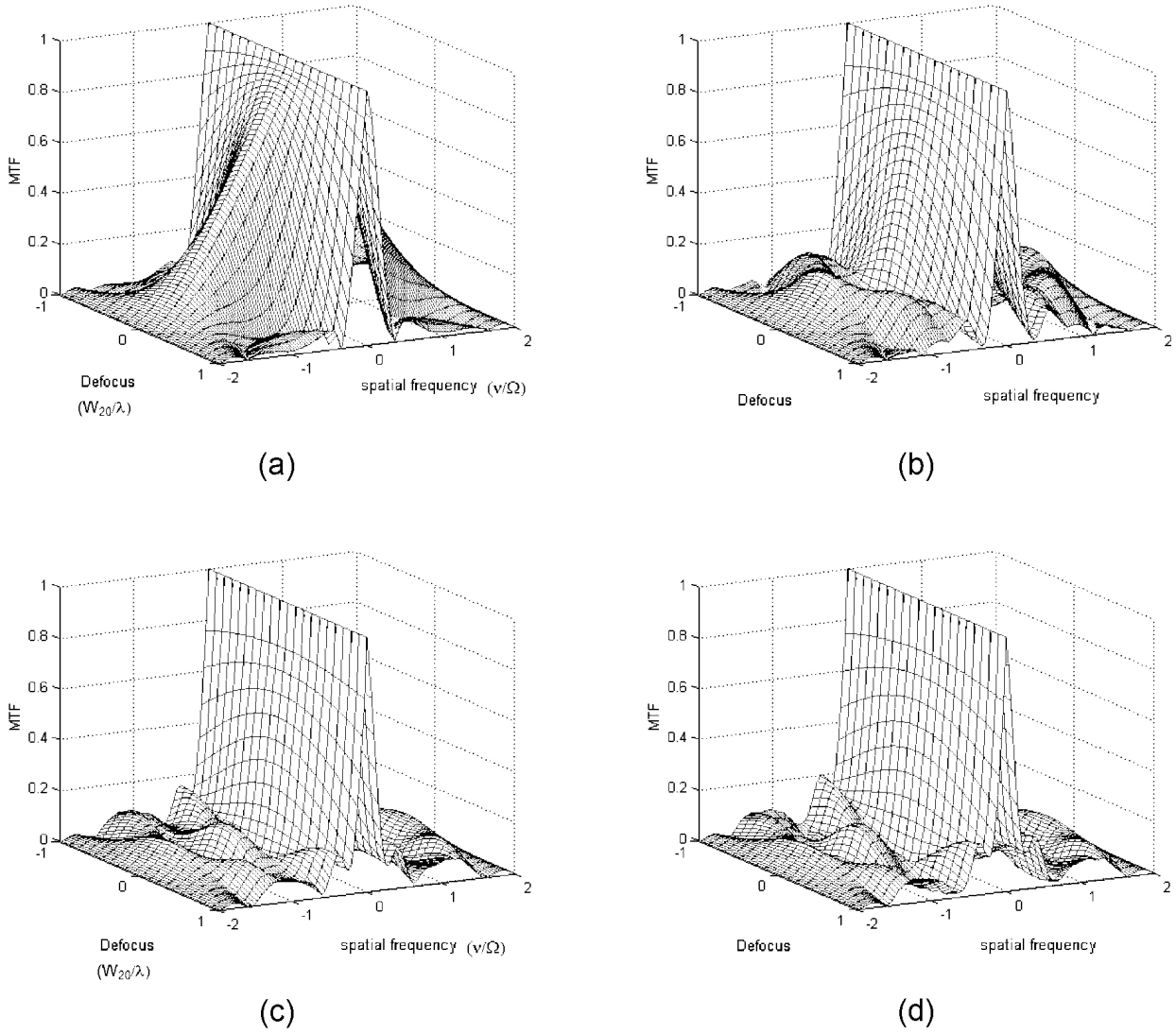

FIGURE 5. 3D-MTF obtained with a system that incorporates the PSAs reported in Ref. 7. (a) ε_1=0, ε_2=0, corresponding to system with the clear circular pupil, (b) ε_1=0, ε_2=0.4, (c) ε_1=0.3, ε_2=0.58, and (d) ε_1=0.35, ε_2=0.62

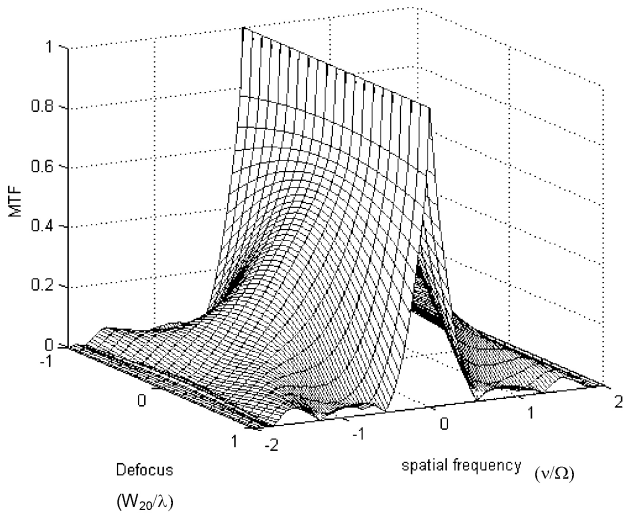

FIGURE 6. 3D-MTF for our proposed PSA with ε_1=0.915, ε_2=1.

Figure 4 presents the simulated images that can be obtained by using the PSAs whose corresponding 3D-MTFs were already studied and presented in Figs. 5 and 6. Along columns in Fig. 4, we show the output images corresponding to three different amounts of defocus: 0, $\lambda/2$ andλ; each row represents a different PSA. Rows 2, 3 and 4 show images with lower contrast and more gray rings than the ones showed in rows 1 and 5, as was expected from the corresponding 3D-MTF (Figs. 5 and 6). We can observe that, for the high frequencies, and severe defocus, $W_{20} = \lambda$, the contrast is decreased in all the cases shown, but in the images of row 5 has a better contrast than for the rest of the PSAs (rows 2, 3 and 4). Regarding the focal depth, images shown in row 5 exhibit better focal depth than the case of row 1. From the images presented in Fig. 4, we corroborate what the 3D-MTF had already predicted: not all the PSAs which exhibit high focal depth are useful for imaging appli-

cations. We can see that, in general, at least the PSAs analyzed here, are not well behaved for imaging applications. However, our proposed PSA, the case presented in the last row of Fig. 4, shows a better optical performance than the rest of them while preserving high focal depth according to its axial impulse response depicted in Fig. 3.

5. Conclusions

The MTF for Phase Shifting Apodizer has been presented and it has been used to evaluate the optical performance from the point of view of optical imaging systems. It has been pointed out that, in imaging applications, it is not enough to synthesize axial impulse responses which exhibit high focal depth. It is necessary to take into account the entire corresponding frequency response of the optical system. We have identified a two-portion phase-shifting apodizer which indeed increases the focal depth and reveals, through its MTF, that it is useful in optical imaging applications.

1. M.D. Levenson, N.S. Viswanathan, and R. Simpson, *IEEE Trans: Electron. Devices. ED*-**29** (1982) 1828.
2. F. Schellenberg, M.D. Levenson, and P.J. Brook. "Optimization of real phase mask performance", Proc. of SPIE **1604**, Annual BACUS Symposium on Photomask Technology, (1991).
3. Naoyuki Ishiwata and Takao Furukawa, "Fabrication of Phase Shifting mask", Proc. of SPIE **1463**, Optical/lase Microlithography IV, (1991).
4. Yuichiro Yanagishita, Naoyuki Ishiwata, Yasuko Tabata, Kenji Nakagawa, and Kasumasa Shigematsu. "Phase Shifting Photolithography Applicable to Real IC Patterns". Proc of SPIE **1463**, Optical/lase Microlithography IV, (1991).
5. M.D. Levenson *et al.*, *IEEE Trans: Electron. Devices. ED*-**31** (1984) 753.
6. H. Ando, *Jpn. J. Appl. Phys.* **31** (1992) 557.
7. H. Wang and F. Gan, *Appl. Opt.* **40** (2001) 5658.
8. H. Wang and F. Gan, *Appl. Opt.* **41** (2002) 5263.
9. Xiumin Gao, Zhou Fei, Wendong Xu, and Fuxi Gan, *Appl. Opt.* **44** (2005) 4870.
10. J.W. Goodman, *"Introduction to Fourier Optics"*, (McGraw-Hill 2^{nd}. Ed., New York, 1968).
11. H.H. Hopkins, *Proc. R. Soc. London Ser. A.* **231** (1955) 91.
12. B.R. Frieden, *J. Opt. Soc. Am.* **57** (1967) 56.
13. C.J.R. Sheppard, *Optik* **72** (1986) 131.
14. C.J.R. Sheppard, *Optik* **74** (1986) 128.
15. C.J.R. Sheppard, M. Cu, and X. Q. Mao, *Opt. Commun.* **81** (1991) 281.